

This is the author-version of a paper published as:
Frost, Ray and Palmer, Sara and Reddy, Jagannadha (2007) Electronic and vibrational spectra of Mn rich sursassite. . *Spectrochimica Acta* 66(2):pp. 312-317

Copyright 2007 Elsevier

Electronic and vibrational spectra of Mn rich sursassite

B. Jagannadha Reddy and Ray L. Frost*

Inorganic Materials Research Program, Queensland University of Technology, 2
George Street, Brisbane, GPO Box 2434, Queensland 4001, Australia

Abstract

The optical spectrum of Mn^{2+} in octahedral coordination for sursassite is characterized by well resolved bands at 580, 515, 470, 390, 340, and 295 nm (17240, 19420, 21280, 25640, 29410 and 33900 cm^{-1}). Crystal field parameters evaluated from the observed bands are $Dq = 690$, $B = 680$ and $C = 2800$ cm^{-1} . A broad band centred around 13000 cm^{-1} attributed to Fe(III) ion is an impurity in sursassite confirmed from EDX analysis. Vibrational spectra have been investigated both by IR and Raman spectroscopy. The correlation between vibrational modes and the structural properties of the manganese silicate, sursassite, is made and compared with other silicates. Two vibrational modes of CO_3^{2-} observed; the antisymmetric stretching mode (ν_3) at 1420 cm^{-1} (IR active) and the out-of-plane bending mode (ν_2) (IR and Raman active) at ~ 875 cm^{-1} . This confirms the Mn rich phases in sursassite as observed from SEM probably a Mn carbonate-rhodochrosite.

Keywords: XRD and SEM analyses, UV-Vis and NIR spectroscopy, sursassite, Mn(II) distorted octahedral symmetry, overtone and combination bands, layered silicates, vibrational spectroscopy

* Author to whom correspondence should be addressed (r.frost@qut.edu.au)
P: +61 7 3864 2407 F: +61 7 3864 1804

1. Introduction

Several natural silicates exist in nature, and many of them occur abundant in a wide variety of geological settings. In addition to being important as ore of Mn metals, they play an active role in the environmental geochemistry and the crystal structures of most are known. Yet a concomitant understanding of their electronic structure is lacking. Geochemically, Mn behaves like Mg, Fe, Ni, and Co and tends to partition into minerals that form in the early stages of magmatic crystallization [1].

A rare manganese and aluminium silicate, sursassite is generally ascribed to the epidote group on the basis of the unit cell dimensions and chemical composition. The ideal formula of sursassite is $\text{Mn}_2^{2+}\text{Al}_3[(\text{SiO}_4)(\text{Si}_2\text{O}_7)(\text{OH})_3]$. The chemical analysis of the mineral shows that the percentage of MnO is about 29 wt%. Sursassite is a monoclinic system with space group $P2_1/m$. The unit cell parameters are $a = 0.870$, $b = 0.579$, $c = 0.978$ nm and $\beta = 108.9^\circ$. Crystal structure data suggests that Mn(II) is in octahedral coordination with the oxygen ligands [2]. The structure and crystal chemistry of pumpellyite are closely related to a number of silicate minerals containing disilicate (sursassite, macfallite) or trisilicate groups (ardennite, orientite). The crystal structure of $\text{Mg}_8(\text{Mg}_2\text{Al}_2)\text{Al}_8\text{Si}_{12}(\text{O},\text{OH})_{56}$ Pumpellyite was modelled in space group $P2_1/m$ with its cell parameters; $a = 0.8576$, $b = 0.5730$, $c = 1.8538$ nm, $\beta = 97.691^\circ$ [3]. The general formula is commonly indicated as $\text{W}_8\text{X}_4\text{Y}_8\text{Z}_{12}\text{O}_{56-n}(\text{OH})_n$, where W are sevenfold-coordinated sites commonly occupied by Ca, X and Y are two crystallographically independent octahedral sites occupied by divalent and trivalent cations, and Z indicates tetrahedral sites invariably occupied by Si [4]. In many cases, it is necessary to supplement powder x-ray diffraction studies with other techniques such as SEM, IR spectroscopy and electron microprobe analysis.

Mn(II) corresponds to $3d^5$ configuration in octahedral coordination has five valence electrons occupying three t_{2g} and two e_g orbitals, i.e. high spin configuration, transitions from ground ${}^6A_{1g}$ state as in the case of divalent manganese/ferric oxide and hydroxide minerals [5-8]. The low spin state (t_{2g}^5 configuration with $S = 1/2$) is normally not observed for Mn(II) [9]. Since all the transitions in d^5 ions are spin forbidden, their intensities are very small. So Mn(II) compounds exhibit pale pink colours. The Mn(II) complexes are generally, fairly ionic due to their zero crystal field stabilization energy [10].

We report here chemical and structural analyses of sursassite originating from New Brunswick, Canada and its full systematic spectroscopic characterization by FTIR, Raman and electronic reflectance spectroscopy in the Vis-NIR.

2. Materials and methods

2.1. Sample preparation

Sursassite, from Strategic Manganese Mine, near Woodstock, New Brunswick, Canada was supplied by Mineralogical Research Co., San Jose, California, USA. The copper rosy coloured crystals of sursassite were extracted from the matrix and used in the present work.

2.2. X-ray diffraction

X-ray diffraction (XRD) patterns were recorded using CuK radiation ($n = 1.5418$) on a Philips PANalytical X' Pert PRO diffractometer operating at 40 kV and 40 mA with 0.125° divergence slit, 0.25° anti-scatter slit, between 3 and 15° (2θ) at a step size of 0.0167° . For low angle XRD, patterns were recorded between 1 and 5° (2θ) at a step size of 0.0167° with variable divergence slit and 0.5° anti-scatter slit.

2.3. SEM analysis

Mineral samples of the sursassite were coated with a thin layer of evaporated carbon and secondary electron images were obtained using an FEI Quanta 200 scanning electron microscope (SEM). For X-ray microanalysis (EDX), three samples were embedded in Araldite resin and polished with diamond paste on Lamplan 450 polishing cloth using water as a lubricant. The samples were coated with a thin layer of evaporated carbon for conduction and examined in a JEOL 840A analytical SEM at 25kV accelerating voltage. Preliminary analyses of the sursassite mineral samples were carried out on the FEI Quanta SEM using an EDAX microanalyser, and microanalysis of the clusters of fine crystals was carried out using a full standards quantitative procedure on the JEOL 840 SEM using a Moran Scientific microanalysis system. Oxygen was not measured directly but was calculated using assumed stoichiometries to the other elements analysed.

2.4. UV-Vis spectroscopy

The UV-Vis spectroscopy is an ideal tool for study of coloured minerals. Spectra of d-d transitions mainly fall in this region and can be studied either by absorption or by reflectance. The technique of reflectance spectroscopy is most suitable for minerals including dark coloured and opaque minerals. A Varian Cary 3 UV-Visible spectrophotometer, equipped with Diffuse Reflectance Accessory (DRA) was employed to record the electronic spectrum of the samples in the region between 200 and 900 nm. This technique allows the study of the reflectance spectra of the samples in the powder form. The DRA consists of a 73 mm diameter integrating sphere, featuring an inbuilt high performance photomultiplier. Sample was mounted on coarse filter paper (# 1), by resuspending the sample and submerging the filter paper into the suspension. Initially a base line was recorded using two pressed polytetrafluoroethylene (PTFE) as reference disks. Next, the sample was mounted flat over the sample port and the reflectance spectrum of the sample, relative to the reference disks, was collected by the integrating sphere. By placing the sample flat any specular components, of reflectance, should be directed out of the DRA entrance port, as the angle of incidence is 0° . The diffuse reflectance measurements were converted into absorption (arbitrary units) using the Kubelka-Munk function ($f(R_\infty) = (1 - R_\infty)^2 / 2R_\infty$). Data manipulation was performed using Microsoft Excel.

2.5. Infrared Spectroscopy

Infrared spectra were obtained using a Nicolet Nexus 870 FTIR spectrometer with a smart endurance single bounce diamond ATR cell. Spectra over the 4000 to 500 cm^{-1} range were obtained by the co-addition of 64 scans with a resolution of 4 cm^{-1} and a mirror velocity of 0.6329 cm/s . Near IR spectra were collected on a Nicolet Nexus FT-IR spectrometer with a Nicolet Near-IR Fibreport accessory. A white light source was used, with a quartz beam splitter and TEC NIR InGaAs detector. Spectra were obtained from $11\ 000$ to 4000 cm^{-1} by the co-addition of 64 scans at a resolution of

8cm^{-1} . A mirror velocity of 1.2659 m/s was used. The spectra were transformed using the Kubelka-Munk algorithm to provide spectra for comparison with absorption spectra. The spectral manipulations of baseline adjustment, smoothing and normalisation were performed using the Spectracalc software package GRAMS (Galactic Industries Corporation, NH, USA). Band component analysis was carried out using the peakfit software by Jandel Scientific. Lorentz-Gauss cross product functions were used throughout and peak fitting carried out until squared correlation coefficients with R^2 greater than >0.995 were obtained.

2.6. Raman microprobe spectroscopy

A small crystal of about 1mm^2 was fixed and oriented on the stage of an Olympus BHSM microscope, equipped with 10x and 50x objectives and part of a Renishaw 1000 Raman microscope system, which also includes a monochromator, a filter system and a Charge coupled Device (CCD). Raman spectra were excited by a HeNe laser (633 nm) at a resolution of 2cm^{-1} in the range; $100\text{-}4000\text{cm}^{-1}$. Repeated acquisition using the highest magnification was accumulated to improve the signal to noise ratio. Spectra were calibrated using the 520.5cm^{-1} line of silicon wafer. In order to ensure that the correct spectra are obtained, the incident excitation light was scrambled. Details of the experimental technique have already been reported [11-12].

3. Results and discussion

3.1. X-ray diffraction analysis

X-ray diffraction patterns of the sursasite and a comparison with the standard reference patterns of sursasite (00-037-0479) and quartz (01-037-0796) are shown in Fig. 1. It is apparent from the XRD patterns that the mineral is sursasite with some minor quartz impurity.

3.2. SEM and BSE images and EDX quantitative analysis of sursasite

Scanning electron microscopy (SEM) and back scattered electron (BSE) images are shown in Figs. 2a and b. Dark areas of the sample are consistent with the monoclinic sursasite phases except for minor amounts of Mg, Ca and Fe. Bright areas are identified as Mn phases (possibly rhodochrosite). Areas where the atomic percentages of Al + Mg + Fe are approximately equal to the silicon atomic percentage is considered to be the pure sursasite phase. The EDX quantitative analyses of the sample were made on different areas; dark (sursasite phase) and bright (Mn rich phase) areas. A set of two selected analyses are shown in Table 1. Analyses of pure phases (black bands) agree closely with the general formula of sursasite, $\text{Mn}^{2+}\text{Al}_3(\text{SiO}_4)(\text{Si}_2\text{O}_7)(\text{OH})_3$ except for the notable presence of Mg, Ca and Fe in the sample studied. The bright areas show variation in composition due to impurities associated with the surfaces of the mineral and are considered to be a Mn rich phases, probably due to Mn carbonate, as well as quartz and fluorphlogopite [$\text{KMg}_3(\text{Si}_3\text{Al})\text{O}_{10}\text{F}_2$]. Ca is seen in all the areas of the sample.

3.3. UV-Vis and NIR spectroscopy

The optical absorption spectrum of Mn^{2+} in octahedral coordination is well-characterized and consists of two broad bands in the 450-600 nm range and a distinctive, sharp band near 408 nm in common minerals [6]. The spectrum of the sample shown in Fig. 3 consists of six bands. Two broad bands of similar intensities at 580 with a component of 550 and 450nm are well defined and two strong bands are located at 515 and 390 nm are the characteristic of divalent manganese in sursassite. The first feature observed at 580 nm (17240 cm^{-1}) is assigned to ${}^6A_{1g}(S) \rightarrow {}^4T_{1g}(G)$ transition and the two intense bands at 515 and 390 nm (19420 and 25640 cm^{-1}) arise from ${}^6A_{1g}(S) \rightarrow {}^4T_{2g}(G)$ and ${}^6A_{1g}(S) \rightarrow {}^4T_{2g}(D)$ transitions. The crystal field states, ${}^4A_{1g}(G)$ and ${}^4E_g(G)$ are independent of Dq and are expected to show sharp bands [13]. Hence the sharp band at 470 nm (21280 cm^{-1}) and relatively sharp band at 450 nm (22220 cm^{-1}) are identified as ${}^4A_{1g}(G)$ and ${}^4E_g(G)$ states. The assignments of the bands are made from the energy levels drawn for d^5 [14] and are presented in Table 2. Energies of the transitions calculated with the parameters $Dq = 690$; $B = 680$; $C = 2800$ and Tree's polarization correction term [15] $\alpha = 90\text{ cm}^{-1}$ find close relation with the observed band energies. There is a discrepancy for the band assigned to ${}^4T_{1g}(F)$ state, might be the effect of Fe(III) impurity. This iron impurity in sursassite causes a broad band in the visible region at 780 nm (12820 cm^{-1}). The ${}^6A_{1g}$ to ${}^4T_{1g}$ band observed for Fe(III) (O/OH)₆ groups in the range 11000 - 13000 cm^{-1} in hematite, goethite, stewartite, and many other silicates [16] and Mn-bearing zoisite (thulite) [17]. The band observed on the higher energy side at 42760 cm^{-1} (210 nm) is due to metal-ligand charge transfer (CT).

The near-IR spectrum of sursassite (Fig. 4) contains bands at 7100, 6450, 5530, 5260, 4420 and 4160 cm^{-1} . Most of these bands are well explained [18-20]. The first feature with two bands in the range 7400 -to- 6000 cm^{-1} is the first OH overtone ($2\nu_1$, $2\nu_3$, and $\nu_1 + \nu_3$). Two bands at 5530 and 5260 are the $\nu_2 + \nu_3$ combination bands of molecular water. A sharp band at 4160 cm^{-1} probably appears due to Si-OH stretching in the isolated Si-OH species. A shoulder to this band at 4420 cm^{-1} is a combination band of the O-H stretching and the Si-OH stretching modes [21].

3.4. IR and Raman Spectroscopy

The vibrational spectra of sursassite are shown in Figs. 5a and b and the corresponding IR and Raman frequencies are given in Table 3. The vibrational spectra can be divided into two regions 3700 - 2500 cm^{-1} where stretching and bending vibrations of water molecules appear. The second region (below 1600 cm^{-1}) includes the vibrations due to the silicate layer and charge-balancing cations [22]. In the first region two bands appear in IR with a sharp band at 3275 and another very broad at 2953 cm^{-1} . These bands shifted to higher wavenumber side at 3335 (with shoulder, 3230) and 2998 cm^{-1} are indicative of hydrogen bonding. An additional sharp band around 3500 cm^{-1} in both the spectra corresponds to hydroxyls not involved in hydrogen bonding [23].

According to the factor group analysis fifty four vibrational bands are expected for silicate layer and charge-balancing cations [22] and the scheme of vibrations are represented as

$$\Gamma_{\text{vib}} = 11A_g(\text{R}) + 13B_g(\text{R}) + 14A_u(\text{R}) + 16B_u(\text{R})$$

Experimentally, 11 IR bands in the region of 1600-600 cm^{-1} were observed (Fig. 5 and Table 3). The number of bands observed is less than half of the number predicted by factor group analysis. This might be due to several reasons: a) IR spectra were unable to obtain below 500 cm^{-1} ; b) In the far-IR range some silicon-oxygen bending and metal-oxygen stretching vibrations may occur [24] and c) accidental degeneracy and very weak intensities of certain modes may also be responsible for the observation of fewer bands. Since most of the IR bands are broad, it is likely that some bands are superimposed to give a broad spectral profile. The observed Raman spectrum contains 13 bands in the region 1600-100 cm^{-1} . The assignments of vibrational bands of sursassite are given in Table 3. The vibrations due to the silicate layer and associated cations follow an order of frequency [24] is given below.

$$\nu_{\text{as}}\text{SiOSi} > \nu\text{SiO}^- > \nu_{\text{s}}\text{SiOSi} > \delta\text{SiO} \text{ and } \nu\text{MO}$$

where $\nu_{\text{as}}\text{SiOSi}$ and $\nu_{\text{s}}\text{SiOSi}$ refer to the asymmetric and symmetric stretching modes of Si-O-Si bridges; νSiO^- represents the stretching modes of terminal Si-O⁻ bonds; δSiO refers to the Si-O-Si and O-Si-O bending modes; and νMO represents the M-O stretching modes. From an early time the IR and Raman spectra of silicates were explored and discussed about the assignments of the bands [23-27]. The assignments of IR and Raman bands in sursassite are given in Table 3 and compared with that of two silicates, silinaite and makatite. The bands between 1300 and 900 cm^{-1} are due to the asymmetric stretching vibrations of Si-O-Si ($\nu_{\text{as}}\text{SiOSi}$) and stretching vibrations of Si-O⁻ (νSiO^-); the band at 822 cm^{-1} might be due to Si(Al)-O in Si(Al)O₄; the bands between 800 and 550 cm^{-1} are assigned to the symmetric stretching vibrations of Si-O-Si ($\nu_{\text{s}}\text{SiOSi}$); the bands below 550 cm^{-1} are due silicon-oxygen bending vibrations and the stretching vibrations arising from M-O bonds. In the present case, bands in the range in the range 1200- 1100 cm^{-1} are not observed. The main bands around 800, 700 and 550 are assigned to the symmetric stretching vibrations of SiOSi. The bending vibrations, δSiO and the metal sensitive low-wavenumber bands are found at ~500, 350, 200 and 150 cm^{-1} . These values agree well with those of silinaite and makatite with slightly different peak positions. One medium intensity IR band at 1420 cm^{-1} and a broad band with weak intensity both in Raman and IR at ~860 cm^{-1} are identified as CO₃²⁻ vibrational modes. This observation confirms the SEM images of Mn rich phases, probably due to Mn carbonate observed in sursassite. The bands in the range of 1400-1500 cm^{-1} correspond to the antisymmetric stretching (ν_3) of CO₃²⁻, and the weak shoulder at ~875 cm^{-1} due to the out-of-plane bending (ν_2) of CO₃²⁻ have been reported from infrared spectroscopy of synthetic calcium silicate hydrates (C-S-H)[28], basic copper carbonate minerals, azurite and malachite [29] and gaspeite, a Ni-Mg carbonate mineral gaspeite [30]. It should be mentioned that the sharp band observed at 353 cm^{-1} arise from Mn(II)-O as has been reported strong absorption for Mn(II) at ~320 cm^{-1} in IR spectra of silicates and compounds with Mn²⁺-O₆ coordination [24].

4. Conclusions

The main reason for the cause of copper rosy colour in sursassite crystals is Mn(II). The effect of Fe(III) resulted in a broad band absorption in the region of 670-890 nm which narrowed down the transmission band width to 30 nm around 650 nm. The optical spectrum of sursassite confirms Mn(II) in distorted octahedral coordination in the complex. Crystal chemical analyses revealed variation in composition due to the notable impurities of Mg, Fe and Ca in sursassite. IR and Raman spectra of sursassite show a complexity of bands in the low wavenumber region $< 1300\text{ cm}^{-1}$ includes the vibrations due to the silicate layer and charge-balancing cations.

Acknowledgements

The financial and infra-structure support of the Queensland University of Technology (QUT), Inorganic Materials Research Program is gratefully acknowledged. We thank the Australian Research council (ARC) for funding the facilities used in this research work. On of us, B. J. Reddy is grateful to QUT for the award of a Visiting Fellowship.

References

- [1] L.A.J. Garvie, P.R. Buseck, *Am. Mineral.* 84 (1999) 946.
- [2] M. Mellini, S. Merlino, M. Pasero, *Phys. Chem. Mineral.* 10 (1984) 99.
- [3] G. Artioli, P. Fumagalli, S. Poli, *Am. Mineral.* 84 (1999) 1906.
- [4] E. Passaglia, G. Gottardi, *Can. Mineral.* 12 (1973) 219.
- [5] R.G. Burns, *Mineralogical Applications of Crystal Field Theory*, Cambridge University Press, Cambridge, 1993.
- [6] P.G. Manning, *Can. Mineral.* 9(1968) 348.
- [7] G.R. Rossman, *Am. Mineral.* 61 (1976) 394.
- [8] D.M. Sherman, T.D. Waite, *Am. Mineral.* 70 (1985) 1262.
- [9] A.S. Marfunin, *Physics of Minerals and Inorganic Materials*. Springer-Verlag, Berlin, 1979, p215.
- [10] A.B.P. Lever, *Inorganic Electron Spectroscopy*, Elsevier Pub., Amsterdam, 1984, p448.
- [11] R.L. Frost, R.L. Weier, *J. Raman Spectrosc.* 34 (2003) 776.
- [12] R.L. Frost, R.L. Weier, *Thermochim. Acta* 409 (2004)79.
- [13] C.J. Ballhausen, *Introduction to Ligand Field Theory*, Mc-Graw Hill Book Company, New Delhi, 1962.
- [14] Y. Tanabe, S. Sugano, *J. Phys. Soc. Japan*, 9 (1954) 753.
- [15] W. Low, G. Rosengarten, *J. Mol. Spectrosc.* 12 (1964) 319.
- [16] G.R. Rossman, *Mineral. Spectrosc.*5 (1996) 23.
- [17] G.Srinivasulu, B.Madhsudhana, B.J.Reddy, R.Natarajan, P.S.Rao, *Spectrochim. Acta* 48A (1992)1421.
- [18] G.R. Hunt, J.W. Salisbury, *Mod. Geol.* 1(1970) 283.
- [19] K. Langer, O.W. Florke, *Fortschr. Mineral.* 52 (1974)17.
- [20] R.L. Frost, K.L. Erickson, *Spectrochim. Acta* 61A (2005)51.
- [21] P. Yu, R.J. Kirkpatrick, B.Poe, P.F. McMillan, *X. Cong, J. Am. Ceram. Soc.* 82 (1999) 742.
- [22] Y. Huang, Z. Jiang, W. Schwieger, *Can. J. Chem.* 77 (1999) 495.
- [23] V.C. Farmer, *The Infrared Spectra of Minerals*, Mineralogical Society monograph 4, Mineralogical Society, London, 1974, p137.
- [24] A.N. Lazarev, *Vibrational spectra and structure of silicates*. Consultants Bureau, New York, 1972.
- [25] P. Tarte, M.J. Pottier, *A.M. Proces, Spectrochim. Acta* 29A (1973) 1017.
- [26] P. McMillan, *Am. Mineral.* 69 (1984) 622
- [27] S.A. Brawer, W.B. White, *J. Chem. Phys.* 75 (1975)2421.
- [28] P. Yu, R.J. Kirkpatrick, B. Poe, P.F. McMillan, *J. Am. Ceram. Soc.* 82 (1988) 742.
- [29] R. L. Frost, W.N. Martens, L. Rintoul, E. Mahmutagic, J.T. Kloprogge, *J. Raman Spectrosc.* 33 (2002) 252.
- [30] B.J. Reddy, R.L. Frost, *N. Jb. Miner. Mh. Jg.*2004 (2004) 525.

List of Tables

Table 1 Atom percentage of elements in sursassite

Table 2 Observed and calculated energies of the bands with their assignments for Mn(II) in sursassite

Table 3 Vibrational spectroscopy of sursassite- a comparison with other silicates

List of Figures

Fig. 1. XRD pattern of sursassite.

Fig. 2. Secondary electron images of sursassite crystals a) SEM and b) BSE.

Fig. 3. Optical spectrum of Mn(II) in sursassite.

Fig. 4. Near-infrared spectrum of sursassite.

Fig. 5. Vibrational (IR and Raman) spectra of sursassite: a) 3700-2500 cm^{-1} region and b) 1600-100 cm^{-1} .

Table 1
Atom percentages of elements in sursassite

Element	Atom percentage	
	Grain 1	Grain 2
Mg	2.27	2.41
Al	22.28	23.46
Si	29.83	30.99
P	0.12	0.09
Ca	2.99	3.36
Mn	40.72	38.09
Fe	1.79	1.60

Table 2

Observed and calculated energies of the bands with their assignments for Mn(II) in sursassite

Observed		Calculated	Transition from ${}^6A_{1g}(S)$
λ (nm)	ν (cm^{-1})	ν (cm^{-1})	
780*	12820*		${}^4T_{1g}(G)^*$
720c*	13890c*		„
580	17240	17022	${}^4T_{1g}(G)$
550c	18180c		„
515	19420	20584	$T_{2g}(G)$
470	21280	22565	${}^4A_{1g}(G), {}^4E_g(G)$
450c	22220c		„
390	25640	24761	${}^4T_{2g}(D)$
340	29410	29231	${}^4T_{1g}(P)$
295	33900	36525	${}^4T_{1g}(F)$
210	47620		CT band

*due to Fe(III); c: component band.

Table 3

Vibrational spectroscopy of sursassite- a comparison with other silicates

IR (cm ⁻¹)		Raman (cm ⁻¹)		Assignment ^a	
Silinaite Reported[22] NaLiSi ₂ O ₅ .2H ₂ O	Makatite Reported[22] Na ₂ Si ₄ O ₉ .5H ₂ O	Sursassite (Present work) Mn ₂ ²⁺ Al ₃ [(SiO ₄) (Si ₂ O ₇)(OH) ₃]	Silinaite Reported[22] NaLiSi ₂ O ₅ .2H ₂ O	Makatite [Reported[22] Na ₂ Si ₄ O ₉ .5H ₂ O	Sursassite [Present work] Mn ₂ ²⁺ Al ₃ [(SiO ₄) (Si ₂ O ₇)(OH) ₃]
3558m(sh)	3563vs	3511m			
3490s	3424vs, br		3472vw		3452s
3396m		3275vs	3389vw	3368vw(sh),br	3335vs
3265m			3259vw	3122w,br	3230s,br
		2953vs,br			2998vs,br
1667m	1679m(sh)		1652vw	1681w	
1639m	1639m				
		1420			
1189s	1429w				
1159s				1244vw	
1111w	1115sh	1178w(sh)			
1042vs(sh)	1089sh		1068vs	1060w	
1026vs	1037vs	1052vs,br		1025s	1086s(vw)
	1007vs		1000w		1026s(vw)
955vs	987s	961s	956w	986w	925vs
	918s	921s		945w	
				919w	
		863s,br			866s

					822s	Si(Al)O
757m	835w 799m 698w	797vs	773w	793w		
	672vw	777vs	734w		705s	
677w	661vw	692s(w)	635s(sh)			
627w	625vw	662s(sh)	609s		618s,br	v _s SiOSi
	564w	609s		567vs	554vs	
535s	518s		501vw			
			490vw	482m	491m	
456vs	460vs		466m	460m		
	436vw		423m	414m		
375m	413s		408m			
	367vw		371m	381w		
339w	355vw		342vw	339vw	353s	δSiO and vMO
	340vw		327m	324m		
	323w		279m	292s	283w	
			259w(sh)	266w		
			250m	226w		
			227m	219w	213s,br	
			196m	194w		
			163m	167w		
			148s	151vw	151s	
			126m	122m		
			107w	100m		

^aAbbreviations: s-strong; vs-very strong; m-medium; w-weak; sh-shoulder; br-broad; v_{as} & v_s-asymmetric& symmetric stretching; δ-bending mode.

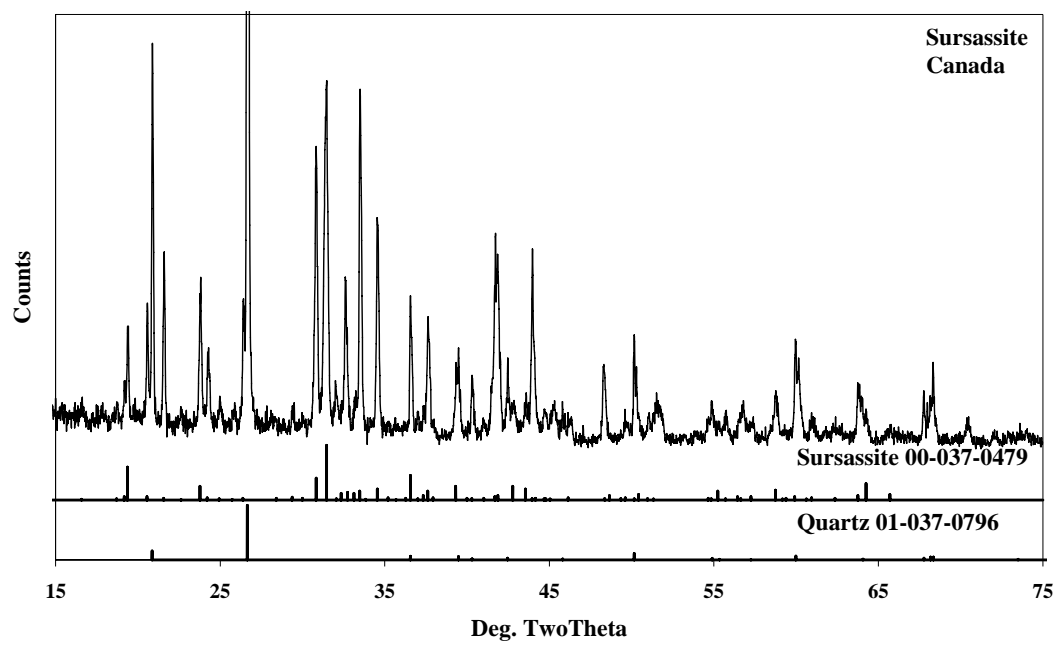


Fig. 1.

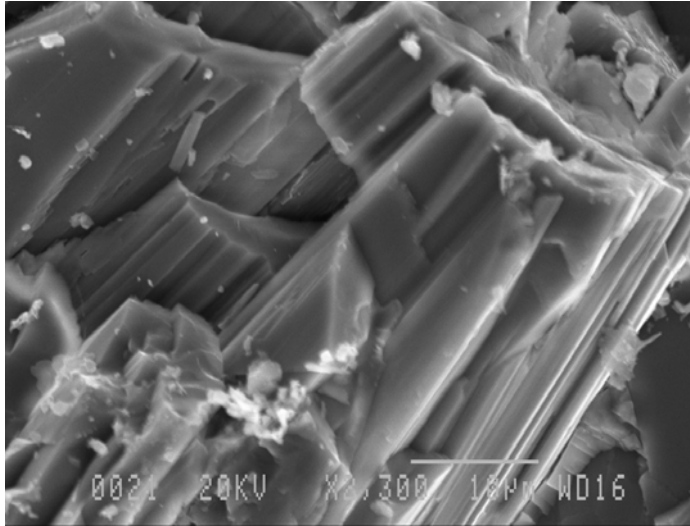


Fig. 2a.

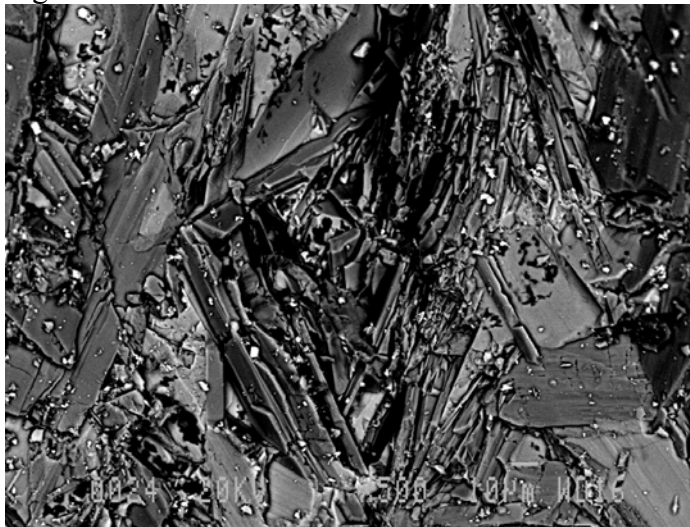


Fig. 2b.

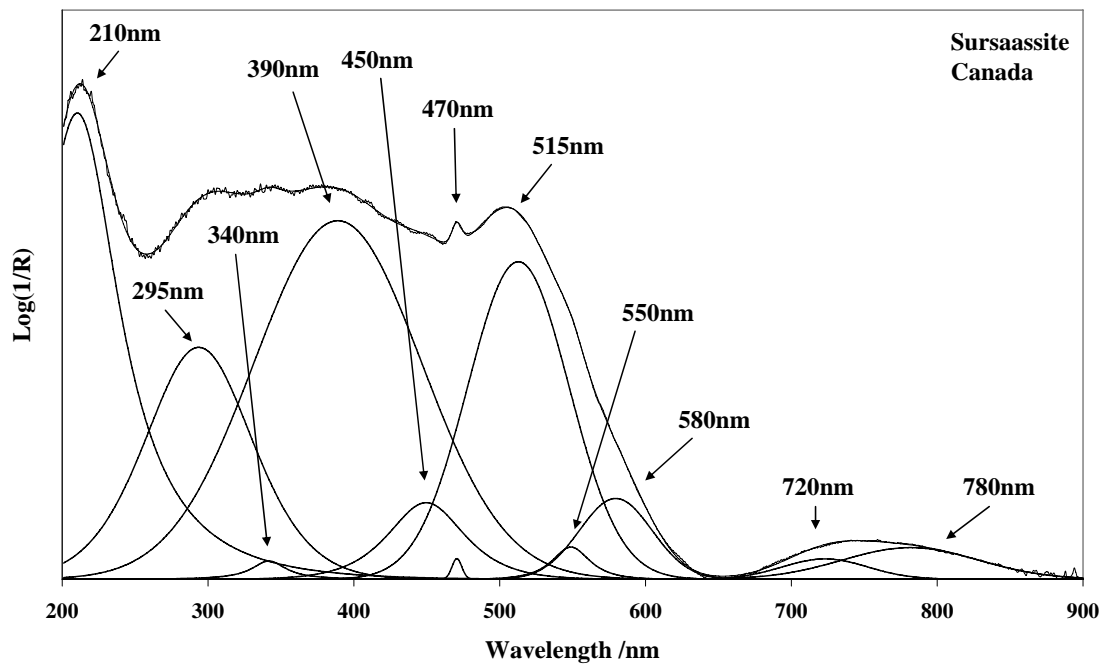


Fig. 3

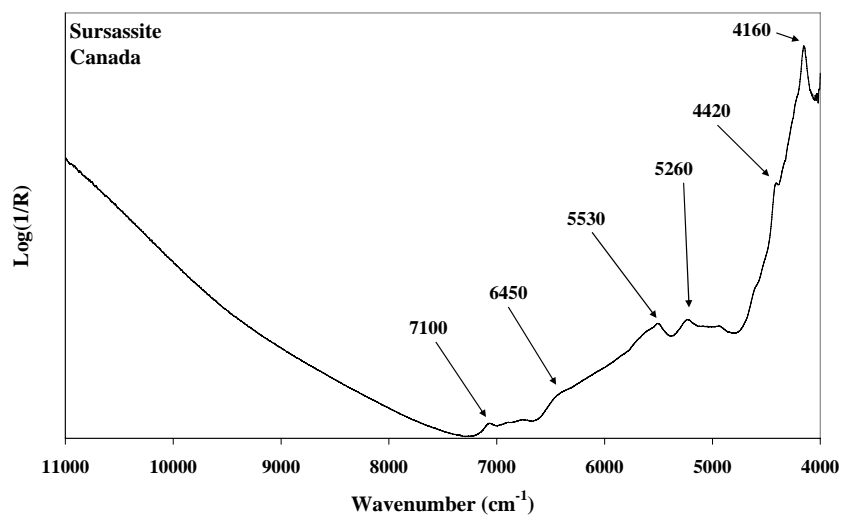


Fig. 4

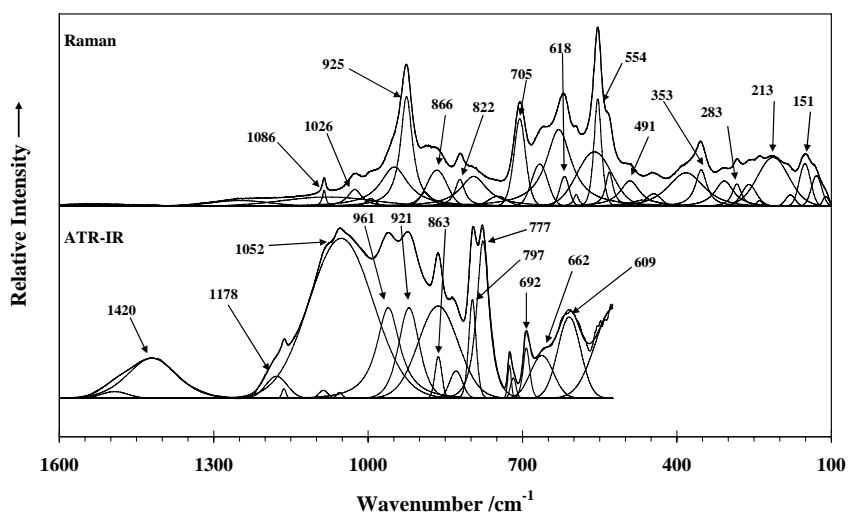
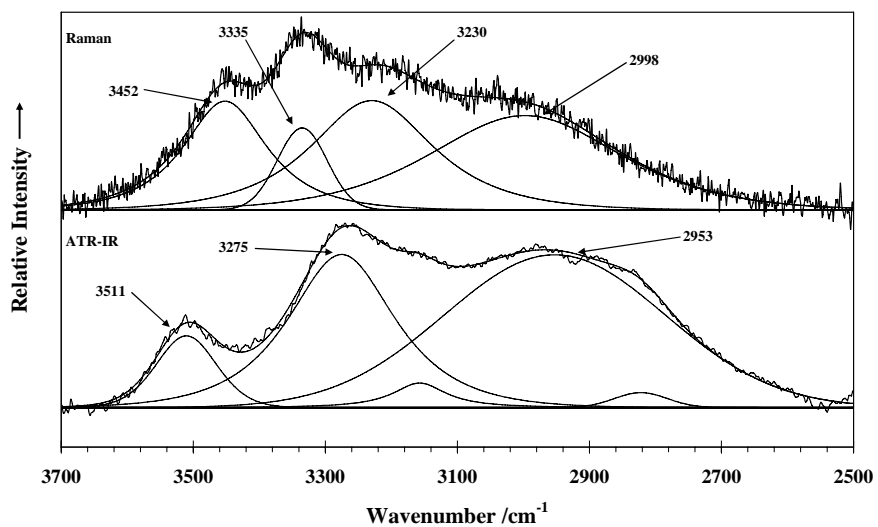


Fig. 5a and b